Experimental analysis of recoverable performance loss induced by platinum oxide formation at the polymer electrolyte membrane fuel cell cathode

M. Zago[a], A. Baricci[a], A. Bisello[a], T. Jahnke[c], H. Yu[b], R. Maric[b,d], P. Zelenay[e], A. Casalegno[a]

[a] Politecnico di Milano, Department of Energy, Via Lambruschini 4, 20156, Milano, Italy

[b] Department of Chemical and Biomolecular Engineering, University of Connecticut, 191 Auditorium Road, Unit 3222 Storrs, CT 06269, United States

[c] German Aerospace Center (DLR), Institute of Engineering Thermodynamics, Pfaffenwaldring 38-40, 70569 Stuttgart, Germany

[d] Department of Materials Science and Engineering, University of Connecticut, Storrs, CT 06269, United States

[e] Materials Physics and Applications Division, Los Alamos National Laboratory, Los Alamos, NM 87545, United States

[*] *Corresponding author:* matteo.zago@polimi.it

Abstract

Unrecoverable and recoverable performance degradation is a major issue hindering commercialization of polymer electrolyte membrane fuel cells. The recoverable losses, caused for example by a contaminant adsorption, catalyst flooding, ionomer dehydration, and platinum oxidation, can be reversed, usually following an interruption in the cell operation. In order to elucidate the link between platinum oxidation and recoverable performance loss, three MEAs were characterized in this work. They involved catalysts with different nanoparticle sizes and loadings tested using a combination of the electrochemical impedance spectroscopy, constant-voltage, constant-current and potential controlled techniques, before and after electrocatalyst aging. Experimental results indicate that a decrease in specific activity over time is not affected by nanoparticle size or aging. Nevertheless, linear sweep voltammetry, which is adopted to

reduce oxide and as diagnostics for oxide composition, reveals that a change in composition is observed in correlation with catalyst morphology and catalyst aging. The formation of the platinum oxide associated with the peak at 0.61 V_{RHE} in the voltammetry is found to decrease the catalyst's specific activity more than oxides associated with peaks at higher potentials. This indicates that the recoverable performance loss due to the oxide formation depends on the oxide composition.

Keywords: aging, polymer electrolyte membrane fuel cell (PEMFC), platinum oxide, recoverable performance loss.

1. Introduction

Polymer electrolyte membrane fuel cells (PEMFCs) are promising future energy-conversion systems in the automotive industry, owing to their low environmental impact, high power density, and efficiency. However, some critical issues, such as performance degradation, must be overcome to facilitate mass commercialization. Studies reported in the literature show that while the PEMFC performance decreases with time under steady-state operation, a fraction of the performance loss can be recovered following a cell shutdown [1,2], which, for this reason, is identified as *recoverable degradation*. The recoverable performance losses have been assigned to various phenomena such as the adsorption of contaminants on the surface of the platinum based catalysts [3]; liquid water flooding of the catalyst layers hindering oxygen access to the active site [4]; dehydration of the ionomer, affecting proton transport and reducing catalyst utilization [1]; and formation of platinum oxides (PtOx) [5]. Unlike the other aforementioned mechanisms, the formation of PtOx cannot be mitigated by optimizing system operative conditions. Even though this phenomenon has been studied extensively in the

literature, its influence on PEMFC operation is not yet fully understood. A brief review of relevant research to date is provided below.

The scientific studies of PtOx in PEMFCs falls under three major topics. The first topic covers the effect of oxides on the mechanism of oxygen-reduction reaction (ORR), which is a complex, multistep electrochemical process that involves numerous surface intermediates. It has been experimentally verified that a transition in the Tafel slope from 60 mV dec^{-1} to 120 mV dec^{-1} is observed at 0.80 V *vs.* RHE. Wang *et al.* [6] demonstrated that this was due to strong adsorption of reaction intermediates, especially the oxygen atom (O) and hydroxide (OH). A recent study confirmed this observation with *operando* X-ray absorption spectroscopy and provided evidence for the presence of dioxygen species (such as OOH) below 0.5 V *vs* RHE [7]. The second topic covers the effect of PtOx on platinum dissolution, which occurs under potential cycling in acidic media. Ahluwalia *et al.* [8] conducted a comprehensive study of Pt dissolution, which included analysis of the complex dependence of dissolution on the nature of the PtOx layer on particles of different sizes. Baroody [9] investigated the formation of a thick oxide layer, to describe platinum dissolution. The last topic deals with the influence of the formation of oxides on recoverable degradation. Uribe *et al.* [5] demonstrated that the Pt activity loss at high potentials could be caused by adsorption of oxygenated species in water and demonstrated that the Pt surface activity could be recovered by pulsing the cell voltage down to 0.20 V.

Despite the significant effort dedicated to this topic, a convergence of opinion has not yet been achieved. Regarding the nature of the oxide, the Jerkiewicz *et al.* [10] concluded that Pt–O was formed below 0.85 V and that place exchange occurred at higher potentials; a similar conclusion was drawn in [11]. In turn, Redmond *et al.* [12], proposed that Pt–O_2 was formed at the expense of an initial oxide species and underwent place exchange. The operando test reported in [13] suggested that Pt–OH could be the oxide responsible for recoverable degradation. It has been accepted in the literature that surface oxides are formed from water, with oxygen playing little

or no role in the oxide formation. Thus, the reaction intermediates involved in the ORR should be of a different nature from that of the oxides that are suspected to have a role in dissolution and recoverable degradation.

Another relevant aspect is that the electro-oxidation of Pt nanoparticles is initiated by surface oxides. However, as the process continues, the oxides become more stable and affect the structure of the nanoparticles [14]. Oxide growth has been known to be logarithmic in time, as reported by Conway and co-workers [15,16]. Moreover the interactions between the catalyst and electrolyte are also known to affect the formation of PtOx, especially as a consequence of the anion-specific adsorption that can reduce the effective active surface [17]. Shinozaki *et al.* [18], using rotating disk electrode methods demonstrated that Nafion lowers ORR activity and that it is also influenced by Pt nanoparticle size [18].

Despite the substantial effort dedicated to both PtOx formation and ORR kinetics, the quantification of the recoverable performance loss during cell operation has not been performed. This is due to the difficulties in extending the literature results, obtained on single crystals, with liquid electrolytes, or at potentials higher than 1.0 V, to actual fuel cell operating conditions. This work aims to demonstrate and characterize the correlation between the voltammetric charge attributed to the PtOx, and the recoverable performance loss, and thereby to elucidate the roles of the nanoparticle size and catalyst aging. The experimental methodology is reported in Section 2. In Section 3, the results are discussed and the origin of the recoverable performance loss is analysed considering the effect of operating conditions.

2. Experimental

2.1 MEA properties

Three 25 cm^2 MEAs, with different properties were tested: a commercial MEA manufactured by EWII Fuel Cell A/S (named EWII for short) and two low-Pt MEAs prepared by the reactive spray

deposition technology (RSDT). As reported by Yu *et al.* [19], the RSDT process allows for a real-time control of the support, catalyst, and ionomer compositions in the electrode. In this work, 3 nm and 5 nm Pt nanoparticles were deposited and the corresponding MEAs were named RSDT 3 nm and RSDT 5 nm, respectively. The properties of the MEAs are listed below:

- RSDT 3 nm: Cathode catalyst loading was 0.05 mg cm^{-2} (3 nm Pt nanoparticles deposited on Ketjenblack), with ionomer-to-carbon ratio of 1 and electrode thickness of 12 μm; anode catalyst loading was 0.05 mg cm^{-2} (Pt) and the membrane was Nafion® 212. Both anode and cathode diffusion layers were Sigracet® SGL25BC (thickness 235 μm, 5% PTFE content, with microporous layer - MPL).
- RSDT 5 nm: Cathode catalyst loading was 0.1 mg cm^{-2} (5 nm Pt nanoparticles deposited on Ketjenblack), with ionomer-to-carbon ratio of 1 and electrode thickness of 12 μm; anode catalyst loading was 0.05 mg cm^{-2} (Pt) and the membrane was Nafion® 212. Both anode and cathode diffusion layers were Sigracet® SGL25BC.
- EWII[1]: Cathode catalyst loading was 0.6 mg cm^{-2} (Pt nanoparticles deposited on low surface-area carbon) and anode catalyst loading was 0.2 mg cm^{-2}.

The reason of employing MEAs with different properties and Pt loading is to extend the validity of the experimental results: in this way it is possible to highlight common phenomena not affected by the characteristics of a specific MEA.

2.2 Experimental setup

The experimental setup used in fuel cell testing was designed and assembled in-house, as described in [20]. The MEA was tested in a 25-cm^2 cell hardware assembly (Fuel Cell Technologies Inc.) with triple serpentine graphite flow-field at both the cathode and anode. The

[1] No further detail can be revealed for confidentiality reasons.

fuel cell voltage was measured using an electronic load and high-precision acquisition board (estimated uncertainty: 1 mV). The flow rates of the reactants were controlled and measured using two calibrated flow controllers (uncertainty: 0.7% of rate + 0.004 Nl min^{-1} for the air flow controller and 0.7% of rate + 0.001 Nl min^{-1} for the hydrogen flow controller). The fuel cell temperature was measured using a thermocouple (uncertainty 0.2 K). The dew point of the feed gas (hydrogen 99.9999%, oxygen 99.999%, or nitrogen 99.9999%) was controlled by means of temperature-controlled humidity bottles (Fuel Cell Technology Inc.). The test station was equipped with a potentiostat with a current booster (up to 10 A) and a DC electronic load, capable of performing electrochemical impedance spectroscopy.

2.3 Experimental tests

This section pertains the description of MEAs testing. Four protocols were performed and were identified with a progressive number. Each protocol, described in Tab. 1-4, consists of a sequence of procedures:

- protocol #1 (Table 1) focused on the analysis of recoverable performance loss under fully humidified hydrogen/oxygen feed at constant cell voltage;
- protocol #2 (Table 2) aimed at finding a correlation between specific ORR activity loss and oxide formation, elucidating the roles of the nanoparticle size and catalyst aging, induced by accelerated stress test (AST);
- protocol #3 (Table 3) was conceived to compare the effect of potential holding and potential cycling on oxide formation and recoverable performance loss;
- protocol #4 (Table 4) focused on the analysis of recoverable performance loss under dry hydrogen/air feed at constant cell current, condition that is more representative of real operation.

The description of each experimental procedure is described in the following.

Step	Name	Description / repetitions
#1	Cell conditioning	
#2	Overnight-off	
#3	Constant voltage under H_2/O_2	Step #3 repeated 2 times, applying constant voltage 0.85V and 0.70V
	EIS	
	Oxygen interruption	
	EIS	
	Overnight-off	

Tab. 1 – List of procedures for protocol #1.

Step	Name	Description / repetitions
#1	Cell conditioning	
#2	Overnight-off	
#3	Constant voltage under H_2/O_2	0.85V constant voltage operation
	Overnight-off	
#4	Constant potential under H_2/N_2	Step #5 repeated 5 times, changing holding time (10s, 30s, 60s, 300s, 9000s)
	LSV - oxide stripping	
	5 minutes at low potential (H_2/N_2)	
#5	Overnight-off	
#6	Accelerated stress test	
#7	Overnight-off	
#8	Constant voltage under H_2/O_2	0.85V constant voltage operation
	Overnight-off	
#10	Constant potential under H_2/N_2	Step #10 repeated 5 times, changing holding time (10s, 30s, 60s, 300s, 9000s)
	LSV - oxide stripping	
	5 minutes at low potential (H_2/N_2)	

Tab. 2 – List of procedures for protocol #2.

Step	Name	Description / repetitions
#1	Cell conditioning	
#2	Overnight-off	
#3	Potential cycling under H_2/N_2	Step #3 repeated 3 times, with 0, 10, 100, 1000 cycles
	LSV - oxide stripping	
	5 minutes at low potential (H_2/N_2)	
#4	Overnight-off	
#5	Potential cycling under H_2/N_2	Step #5 repeated 3 times, with 0, 10, 100, 1000 cycles
	Switch to H_2/O_2	
	Constant voltage under H_2/O_2	0.85V constant voltage operation
	Switch to H_2/N_2	
	LSV - oxide stripping	
	5 minutes at low potential (H_2/N_2)	

Tab. 3 – List of procedures for protocol #3.

Step	Name	Description / repetitions
#1	Cell conditioning	
#2	Overnight-off	
#3		Step #3 repeated 4 times after different recovery strategies
	Recovery procedures	Described in the text (section 3.4)

Tab. 4 – List of procedures for protocol #4.

2.3.1 Cell conditioning

Cell conditioning was performed according to previous works by the authors [19,21]. It consisted in 20 voltammetric scans between 0.05 V and 1.0 V at 20 mV s^{-1} at room temperature, then at 80°C under fully humidified H_2/N_2 feed. After this period, the sample was run at constant voltage (0.6 V) under H_2/air with stoichiometry 2 for both reactants. This operation was stopped after a stable current output was measured, typically achieved within 6-8 hours.

2.3.2 Overnight-off

Overnight, the sample was maintained at 80°C temperature with fully humidified H_2/N_2 gas feed. This procedure was applied for approximately 14 hours.

2.3.3 *Constant voltage under* H_2/O_2

The sample was operated at constant voltage (0.85 V or 0.70 V) under fully humidified H_2/O_2 gas feed (stoichiometry 2 and 9.5) and the fuel cell temperature was set at 80 °C. These conditions were properly adopted to emphasize the catalyst ORR activity.

2.3.4 *Electrochemical impedance spectroscopy*

Electrochemical impedance spectroscopy (EIS) was performed at constant current, equal to the value measured at the beginning of the procedure (if constant voltage operation was applied before). EIS was performed in the frequency range between 10 kHz and 0.1 Hz and a small current amplitude was selected to have a voltage oscillation around 10 mV or less.

2.3.5 *Oxygen interruption*

This procedure consisted of closing the oxygen feed to the cell while keeping the hydrogen feed open. Consequently, the cell voltage started to slowly decay because of hydrogen crossover consuming oxygen at cathode catalyst layer. After voltage declined below 0.30 V, this condition was maintained for 60 s.

2.3.6 *Constant potential under* H_2/N_2

Potential holding was performed under fully humidified inert conditions (H_2/N_2, 50/50 ml min^{-1}). Applied potential was 0.85 V_{RHE} and the sensitivity to the holding time was studied using the following time intervals: 10 s, 30 s, 60 s, 300 s, and 9,000 s.

2.3.7 *Potential cycling under* H_2/N_2

This procedure was applied under fully humidified inert conditions (H_2/N_2, 50/50 ml min^{-1}) and consisted of potential cycling between 0.85 and 0.70 V_{RHE} at a scan rate of 0.05 V s^{-1}. This

test was performed with a different number of cycling: 0 (meaning no cycles), 10, 100, and 1,000.

2.3.8 Linear sweep voltammetry – oxide stripping

A linear sweep voltammetry (LSV) was performed under H_2/N_2 gas feed to study the oxide charge covering the catalyst. LSV started from 0.85V and stopped at OCV potential (0.085 V). Assuming that only PtO was formed and that the number of electrons n_e involved in the reaction was 2, the corresponding coverage could be evaluated from the LSV using the following equation [35]:

$$\theta_{PtO} = \frac{\int_{V_{dl}}^{V_{\max}} i \cdot dV}{sr \cdot \sigma_m \cdot L_{pt} \cdot n_e \cdot ECSA}, \quad (1)$$

where V_{max} is the upper potential limit, V_{dl} is the potential corresponding to the local maximum of the double-layer current, σ_m is the hydrogen charge density of 210 μC cm^{-2}, sr is the sweep rate (mV s^{-1}), L_{Pt} is the platinum loading (mg_{Pt} cm^{-2}) and ECSA is the electrochemical active area (m^2 g^{-1}). As already reported in the literature for the study of Pt oxidation with potential controlled techniques, the choice of a reference oxide is necessary for data visualization and typically PtOH or PtO are selected [22]. This was done since the separation between different oxides is not trivially done. In this work, PtO basis was adopted in order to avoid a coverage value higher than 1, which would happen using PtOH basis. It is to be observed that the adoption of reduction charge or the assumption of single oxide species does not alter the presented results.

The ECSA[2] value reported in Eq. (1) was evaluated from the hydrogen desorption peak, calculated as:

[2] The definition of ECSA refers to MEA platinum loading at BOL.

$$ECSA = \frac{\int_{V\min}^{V_{dl}} i \cdot dV}{sr \cdot \sigma_m \cdot L_{pt}}, \quad (2)$$

where V_{min} is the lower potential limit and V_{dl} is the potential corresponding to the local minimum of the double-layer current.

2.3.9 Accelerated stress testing

The AST was performed according to the protocol defined by the U.S. Department of Energy to selectively accelerate electrocatalyst degradation. The protocol involved a triangular potential sweep between 0.6 and 1.0 V *vs.* DHE at 50 mV s^{-1} while feeding fully humidified H_2/N_2 (0.05/0.05 Nl min^{-1}) at 80 °C, in accordance with [34]. This protocol was purposely designed to induce Pt dissolution and Pt nanoparticle growth. In order to compare the samples at end of life (EOL) with similar ECSA, the three MEAs were subjected to a different number of AST cycles[3]: 5,000 (RSDT 3 nm), 10,000 (RSDT 5 nm), and 30,000 (EWII).

2.3.10 Cathode feed gas switch

In the cathode gas feed, two parallel pipelines were connected. Each had a flow meter and a bubbler. Cathode feed gas was switched from O_2 to N_2 (or the opposite) by opening/closing the flow meter valve, in order to have fast replacement of gas composition.

2.3.11 Constant current under H_2/Air

The fuel cell was operated at 0.5 A cm^{-2} and the temperature was fixed at 65 °C. The anode and cathode were fed with hydrogen (stoichiometry 2, relative humidity 30%) and air at ambient pressure (stoichiometry 2, relative humidity 20%), respectively.

[3] The same samples were previously tested under the same AST up to 30,000 cycles and thus the proper number of cycles was already known. The applied AST cycles number is justified by the different nanoparticle size and distribution.

3. Results and discussion

3.1 Electrochemical origin of recoverable performance loss

In this section, a preliminary analysis is reported to elucidate the electrochemical origin of a relevant fraction of recoverable performance loss. The presented results have been obtained following the experimental protocol #1, that was applied only on a new MEA RSDT 3 nm. Fig. 1 illustrates constant-voltage operation at both 0.85 V and 0.70 V.

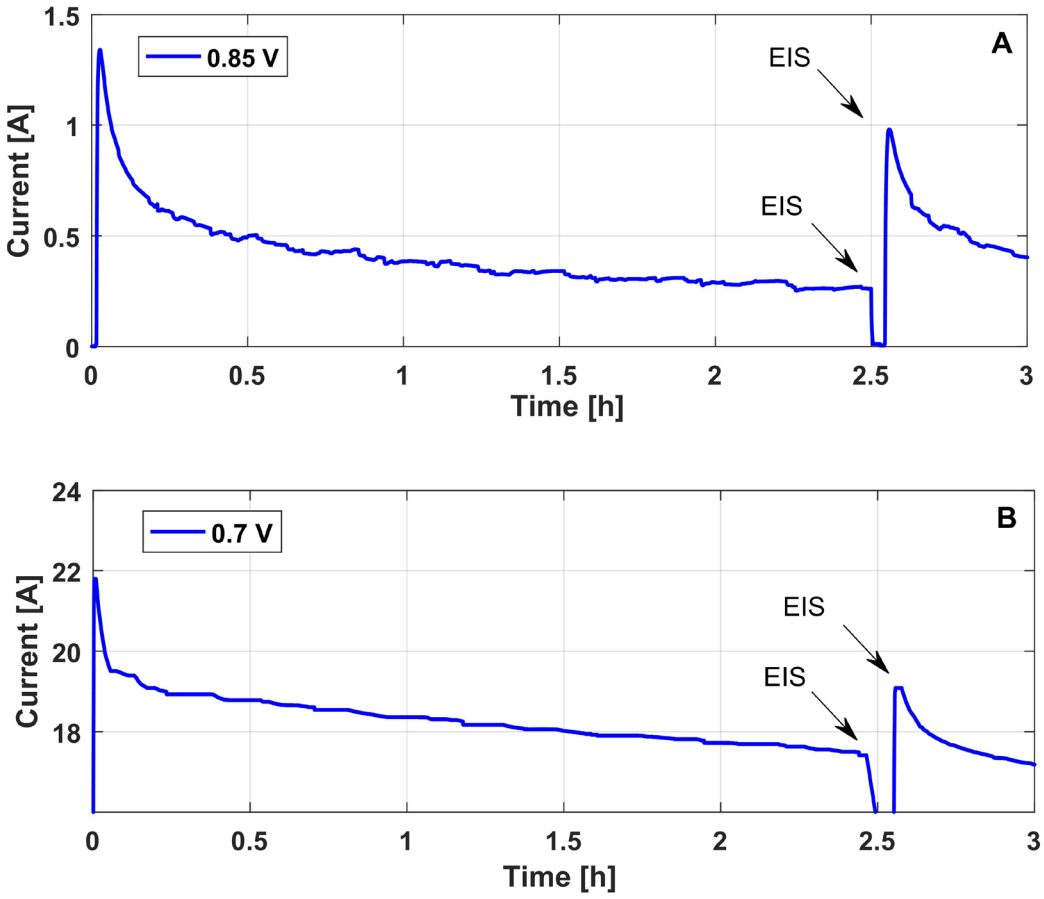

Fig. 1 – Evolution of current during constant-voltage operation, for MEA RSDT 3 nm: (A) voltage hold at 0.85 V; (B) voltage hold at 0.70 V.

The constant-voltage operation at 0.85 V resulted in a considerable reduction in the current with time. The current decreased to 20% of its initial value after two and a half hours. A similar trend in the performance loss was observed during a voltage hold at 0.70 V, however quantitatively lower than the previous case, reaching 80% of initial value of current after two

and a half hours of testing. Even though there was a quantitative difference between the experiments at 0.85 V and 0.70 V, a logarithmic trend was observed in both cases, indicating that the same physical cause is behind this obeservation. After one minute at a cell voltage lower than 0.30 V_{RHE}[4], a considerable but incomplete recovery of performance was observed: the current reached 65% for the test at 0.85 V and 85% for the test at 0.70 V (percentage is referred to the value at time zero).

The analysis of EIS performed before and after[5] the recovery procedure (Fig. 2) does not show any change in the high-frequency region, confirming that the ionic conductivity of the membrane and ionomer did not vary because of dehydration.

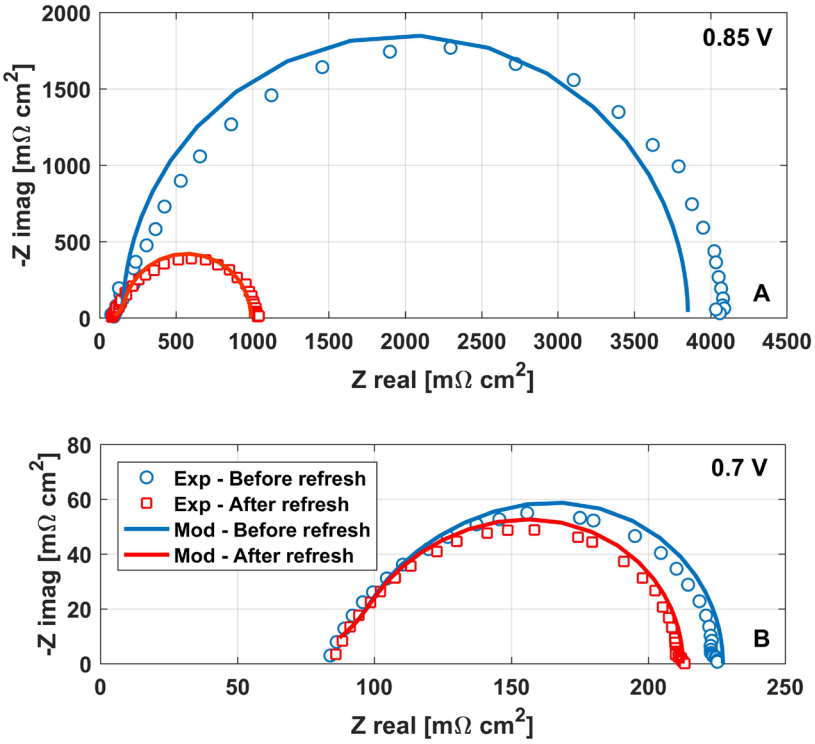

Fig. 2 – Comparison between simulated and measured EIS before and after recovery procedure: (A) voltage hold at 0.85 V; (B) voltage hold at 0.70 V.

[4] This was performed by interrupting the oxygen feed and carefully reducing the cell voltage difference. One minute represents only the time during which the voltage is lower than 0.30 V.

[5] After recovery procedure (operation at 2.5 h in Fig. 1) the cell operation is not in steady-state. In order to limit issues on EIS reliability, the impedance spectrum was recorded in 7 minutes, most of which required for the lowest frequency (0.1 Hz).

Moreover, the shape of the spectrum was close to an ideal semicircle, typical for a process dominated by a charge-transfer reaction with negligible mass-transport effects, which was in agreement with H_2/O_2 gas feeding. The charge-transfer resistance changed considerably at 0.85 V because of a significant current decrease (Fig. 1A); accordingly, at 0.70 V, the variation of the spectrum as well as the current decrease were minor (Fig. 1B).

In the investigated operating condition, the performance loss is not affected by oxygen or ion transport. In the next sections, additional elements are presented to link this performance loss to the formation of the superficial PtOx coverage that reduces the active area available for the ORR, thereby lowering fuel cell performance.

The physics-based model of electrochemical impedance presented in [23] was used in confirming that the recovery of catalyst active area determines the change in the spectra observed from experiments. Model parameters are reported in Table 5, where the assumed values and those provided by calibration are indicated.

$\delta_{CL,C}$	12	µm	Assumed
$\delta_{CL,A}$	5	µm	Assumed
δ_M	40	µm	Assumed
φ_{CL}	0.6	-	Assumed
σ_M	5	S m^{-1}	Fitted on high frequency resistance EIS
σ_{CL} @ 0.7 V	1.6	S m^{-1}	Fitted on EIS
σ_{CL} @ 0.85 V	0.8	S m^{-1}	Fitted on EIS
α_C @ 0.7 V	0.5	-	Assumed
α_C @ 0.85 V	1	-	Assumed
i^*_C ECSA	7.12	A cm^{-3}	Fitted on potential at 0.05 A cm^{-2}
$C_{DL,C}$	26.4	F m^{-3}	Fitted on bode plot of EIS
α_A	0.5	-	Assumed
i^*_A ECSA	6000	A cm^{-3}	Assumed
$C_{DL,A}$	110	F m^{-3}	Assumed
γ_A	0.25	-	Assumed

Tab. 5 – Assumed and fitted model parameters.

Since the constant-voltage operation was performed at both 0.85 V and 0.70 V and the potential value affects ORR mechanism, for model validation two different transfer coefficients were adopted: 1 for high voltage (0.85 V) and 0.5 for low voltage (0.70 V). These values are in agreement with those discussed in literature [24].

During the EIS simulations before and after the recovery procedure, the value of i^*_C ECSA was changed proportionally to the reported current reduction in order to introduce in the model the formation of superficial PtOx coverage. In this way, the model was able to reproduce the experimental data accurately (Fig. 2); moreover, there was a good agreement between the simulated and measured relaxation frequency (Fig. B.1). Considering that the double-layer capacitance was maintained at constant before and after the recovery procedure, all the main physical phenomena were described correctly, including the deformation of the semicircle towards a linear behavior at high frequencies, due to ion transport limitations through the catalyst layer appearing at 0.70 V.

The simulation results show that the values of the transfer coefficient α and double-layer capacitance did not change during the voltage hold, suggesting that the ORR mechanism was not altered. Therefore, the change in the charge-transfer resistance after the period at low voltage could be attributed exclusively to the current density increase. We can conclude that the current decrease with time as shown in Fig. 1 should be attributed to a temporary reduction of the effective ECSA. In the next section, a correlation withPtOx formation is searched.

3.2 Effect of PtOx formation on performance loss

The results reported in this section have been obtained following the experimental protocol #2 (Tab. 2), that was applied on three fresh MEAs: RSDT 3 nm, RSDT 5 nm and EWII. The evolution

of the specific ORR activity[6] with time at a cathode potential of 0.85 V[7] at the beginning of life (BOL) and after the AST (EOL), is presented in Fig. 3.

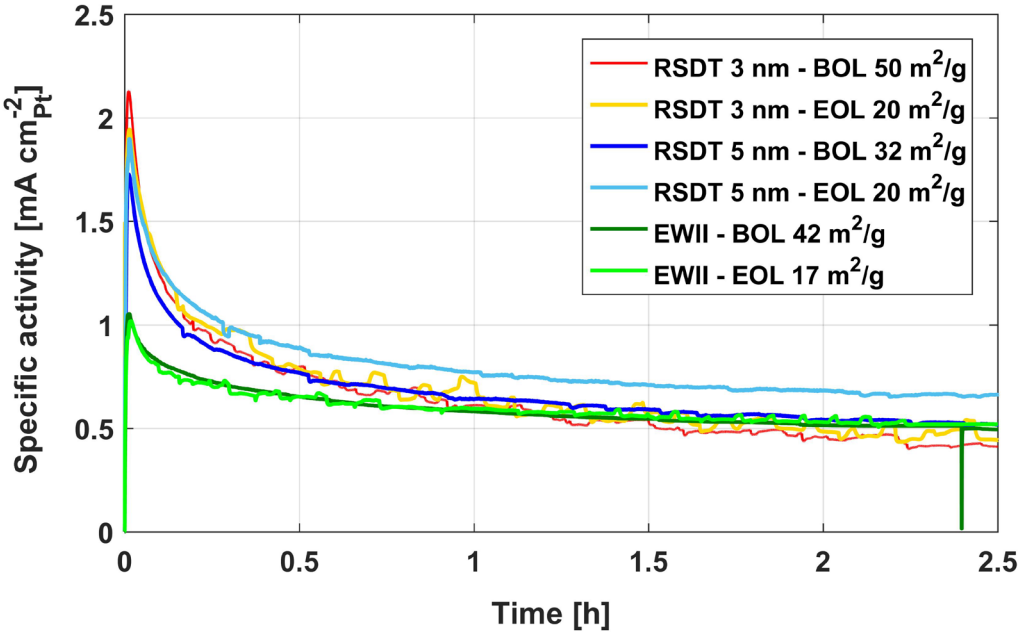

Fig. 3 – Evolution of specific ORR activity with time at 0.85 V for all the tested MEAs (ECSA values given in legend).

The specific ORR activity changed only moderately after inducing nanoparticle growth by AST [8,21], despite a remarkable decrease in the ECSA value is found: the measured values are reported in the legend of Fig. 3. This result agrees with some published research [25] and indicates that the effect of PtOx formation seemed to be substantially unaffected by the ECSA loss that was induced by the AST.

To confirm and explore this result, LSV performed in H_2/N_2 feeding at different holding times are reported in Fig. 4[8], up to 9,000 seconds (corresponding to the duration of the test in Fig. 3). In accordance with the literature [15], the longer the potential hold time is, the higher the oxide

[6] Specific ORR activity is evaluated as the ratio between cell current density and cathode ECSA multiplied by its corresponding catalyst loading.
[7] At a constant-voltage of 0.85 V, the cathode potential can be assumed close to 0.85 V *vs.* RHE. This is because the anode and membrane losses are estimated by the model [23] to be less than 4 mV in the investigated cases, except in the case of EWII MEA at BOL, where it is approximately 6 mV.
[8] The holding at 30 s and 60 s is not reported for the sake of figure readability.

coverage is, thus the higher the measured reduction charge/area in the LSV. On comparing the LSVs at BOL, a strong similarity could be noticed between the RSDT 3 nm and 5 nm samples. The nanoparticle size did not significantly influence the shape of the corresponding voltammograms in the selected range. For a hold time of 10 s, two peaks were evident, whereas one peak dominated the voltammograms recorded after the potential hold for 9,000 s. In the literature, the presence of different peaks was attributed to the formation of a heterogeneous oxide layer, the exact structure and composition of which is still undefined [12].

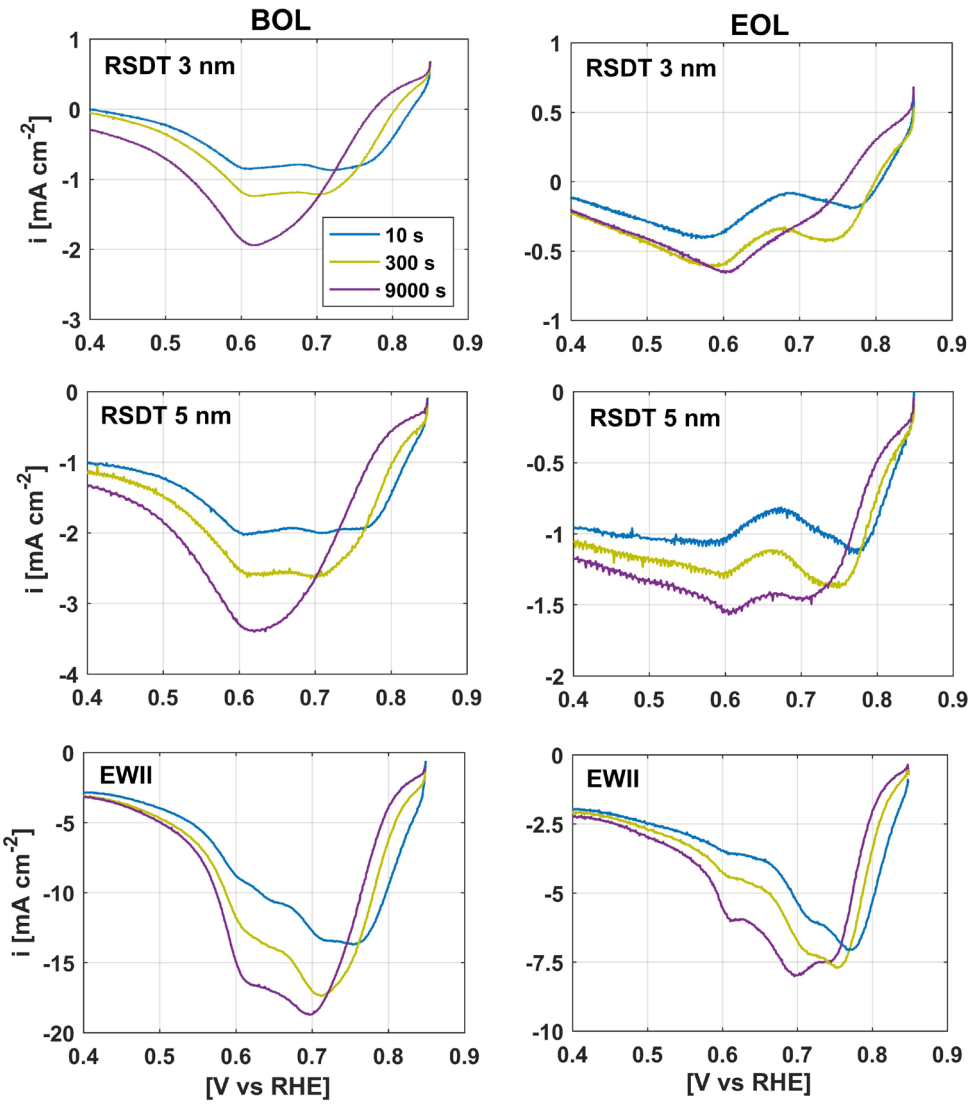

Fig. 4 – LSV at BOL and EOL for different hold times at 0.85 V in N_2: BOL on the left, EOL on the right.

For commercial MEA at BOL, two distinct peaks were always present: the first is visible at 0.61 V_{RHE} and 0.70 – 0.75 V_{RHE}, even after long time holding (9,000s). Instead, one single peak is found after long time potential holding in RSDT 3 nm and RSDT 5 nm samples. When analysing the changes in the LSVs after the AST protocol was applied, a different shape of the voltammogram was observed for all the samples, suggesting the formation of a different composition of oxides after aging. This behavior was more evident for the RSDT MEAs. Interestingly, for all the MEAs, at both BOL and EOL, a peak around 0.61 V_{RHE} is detectable for short holding time (up to 300s). It increased with the time of potential hold, suggesting an existence of a more stable oxide that is formed regardless of the nanoparticle size and catalyst aging. In the case of other peaks, a shift toward lower potential was observed in all the investigated cases upon increasing the potential-hold time. This shift likely indicates the formation of a more stable form of oxide.

A precise quantification of the oxide coverage from LSVs is not possible without the identification of the type the oxide species, *e.g.*, PtOH, PtO, PtO_2, each requiring a different numbers of electrons during the reduction process. The difficult task of identifying surface oxides is out of the scope of this work, consequently, the discussion that follows below is limited to the oxide reduction charges[9], as measured from the LSVs, and the specific ORR activity loss. Consistent PtOx formation during potential holds under different atmospheres, *i.e.* N_2, O_2 and air, is demonstrated in Appendix A.

Fig. 5 combines the charge measured by the LSV at a given holding time (obtained from Fig. 4), with the corresponding value of specific ORR activity (evaluated from Fig. 3).

[9] In the following, the oxide reduction charge is expressed as ECSA coverage under the assumption that the oxide surface species is PtO, calculated from Eq. (1).

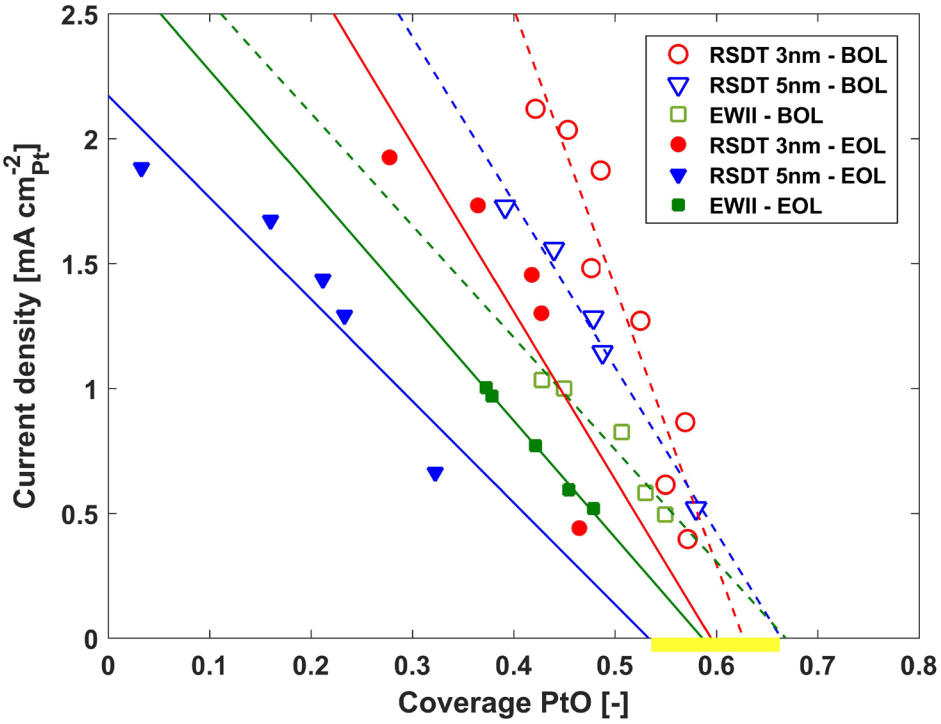

Fig. 5 – Correlation between PtO coverage and specific ORR activity at 0.85 V.

Despite the fact that the oxide composition varied for the three MEAs at BOL and EOL (Fig. 4), it is possible to observe that at specific activity equal to zero (highlighted in the yellow box) all the MEAs present a coverage included between 0.55 and 0.65 (PtO basis), suggesting the persistent presence of one type of oxide regardless of conditions and aging. Focusing on the value of PtOx coverage for which zero ORR activity is found, the tests performed at BOL leaded to a coverage that is higher than 0.6, while a coverage below 0.6 is found for the tests at EoL. This effect that is still limited could also be related to the increased measurement uncertainty in ECSA estimation after ageing. In general, aging apparently induced a shift toward slightly lower PtO coverage and an increase in the negative slope of the fitting line. The EWII MEA showed minor variations, even though its ECSA at EOL was reduced to 40% of its original value. From this analysis, we can state that the relation between PtO coverage and loss of specific ORR activity weakly depends on the properties of the catalyst layer and catalyst aging.

3.3 Influence of PtOx composition on performance decay

As two types of oxides were detected from LSV, which were identified by a potential at which the reducing current peaked, the analysis was expanded to distinguish the effect of each oxide on the specific ORR activity. The results reported in Fig. 6 have been obtained following the experimental protocol #3 (Tab. 3), that was applied on a new EWII MEA. After cycling the cathode potential between 0.70 V_{RHE} and 0.85 V_{RHE} (Fig. 6A), the total measured PtO coverage was almost constant around 0.31 (values reported in the legend). It was evident that a different composition of PtOx was achieved and that the share of the oxide that gives rise to the peak at 0.61 V_{RHE} increased considerably during cycling.

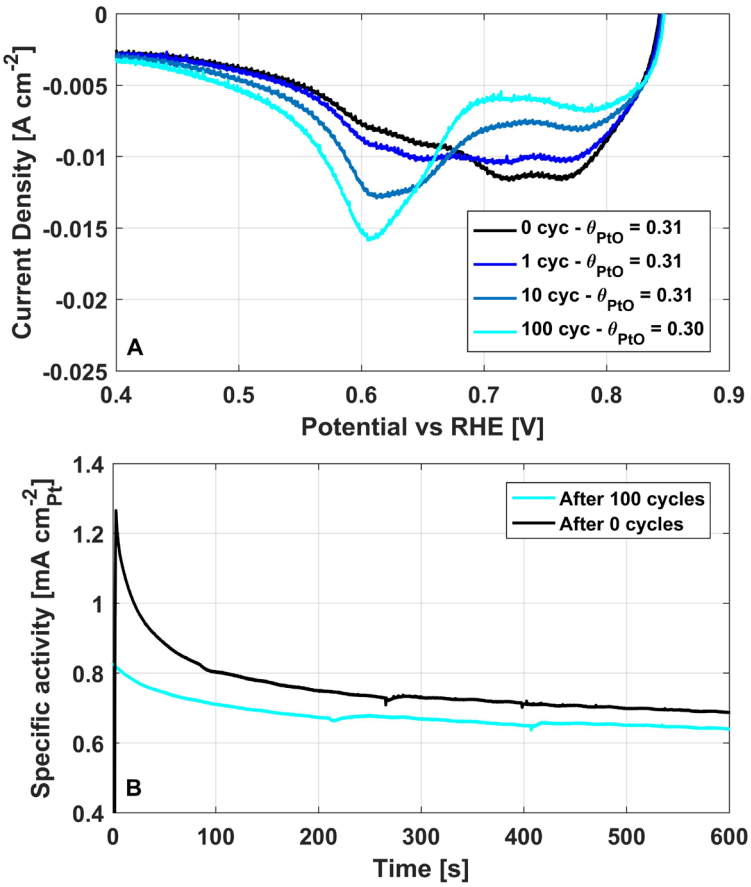

Fig. 6 – Experimental data at BOL after a variable number of potential cycles between 0.85 and 0.70 V_{RHE} for EWII MEA: (A) LSV; (B) specific ORR activity evolution.

In order to isolate the influence of the PtOx composition on the specific ORR activity, after potential cycling in N_2, the oxygen reduction current at 0.85 V was measured to assess ORR

activity of the oxidized catalyst (step #5 of protocol #3 in Tab. 3). The results are reported in Fig. 6.B. Despite the fact that the total coverage at time 0 was the same after 0 and 100 cycles, the specific activity was dramatically reduced after 100 potential cycles. It is concluded that the coverage associated with the peak at 0.61 V_{RHE} hindered the ORR specific activity more significantly than the coverage of other oxides responsible for peaks at higher potential. The reduction of ORR specific activity observed during the potential hold at 0.85 V_{RHE} after cycling was less than that without potential cycling: the specific activities between the two cases after 600 s were similar.

3.4 Influence of PtOx formation during constant-current operation

Up to this point, the operating conditions for all MEAs were chosen to maximize the recoverable performance loss caused by the PtOx formation—high potential and oxygen feed to limit mass-transport losses. However, PEMFCs usually work in constant-current mode for a long time, at a current density between 0.5 and 0.7 A cm^{-2}. Under such a condition, the operating cathode potential is generally lower than 0.75 V and the ion transport limitations associated with ionomer dehydration can play a significant role in determining the system dynamics.

In order to quantify the recoverable performance loss induced by the PtOx coverage under practical conditions, the protocol #4 (Tab. 4) was applied on a new EWII MEA. The cell was operated at 0.5 A cm^{-2} for 200 h and the operation was systematically interrupted to recover performance. The procedures were changed to obtain an insight into the origin of the recoverable performance decay. The measured cell voltage and high frequency resistance (HFR) are depicted in Fig. 7.

The first interruption was performed after 60 h and involved two minutes of operation at 1.2 A cm^{-2}. The previous anode and cathode flow stoichiometries were maintained and the cell voltage during the interruption reached approximately 0.30 V. When the current density was

reset to 0.5 A cm^{-2}, only a partial recovery of performance was observed. At 1.2 A cm^{-2}, a sum of the ohmic and anode losses accounted for approximately 70 mV, resulting in cathode potential of approximately 0.40 V_{RHE}. According to LSV analysis of Fig. 4, by sweeping the potential down to 0.40 V_{RHE} the measured current corresponds to the one associated to the double layer capacitance and therefore all the oxides should be reduced on Pt surface, resulting in full performance recovery.

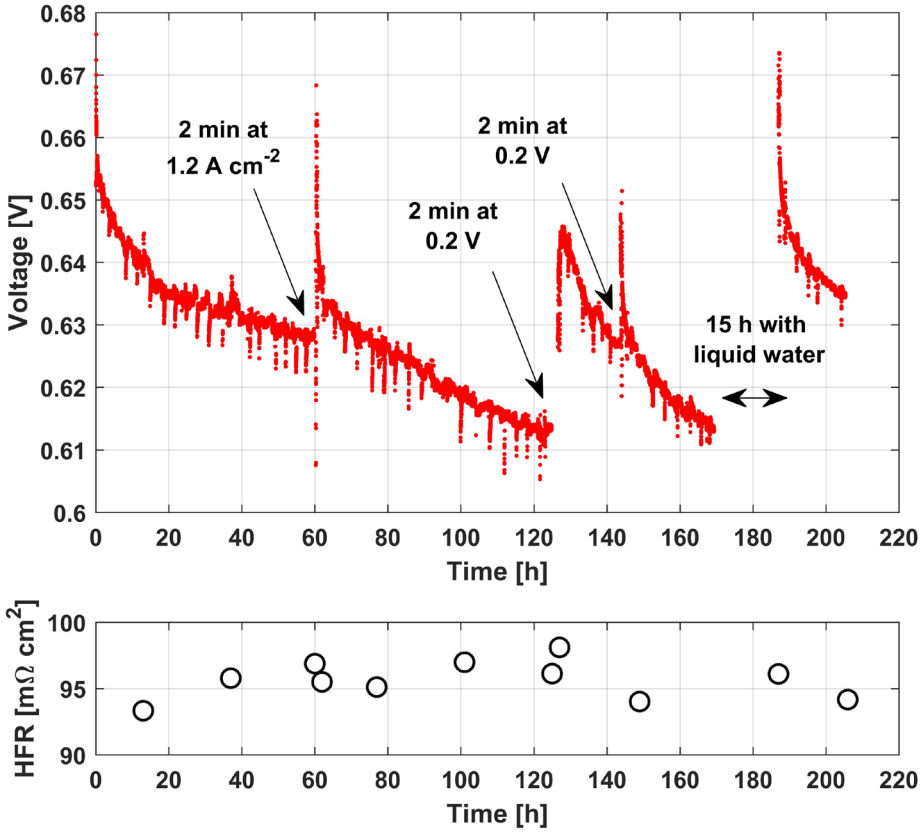

Fig. 7 –Cell voltage and HFR of EWII MEA during constant-current hold at 0.5 A cm^{-2} interrupted by different recovery procedures.

Subsequently the cathode potential was lowered further with a different recovery procedure applied after 120 h of operation. Similarly to the oxygen interruption procedure (section 2.3.5), the air feeding was stopped. The cell voltage (cathode potential) dropped to 0.20 V and was maintained for two minutes, then operation at 0.5 A cm^{-2} was restored. The performance recovery was higher than that achieved at 60 h by applying high current density, even though

a complete recovery was not obtained in this case either. Thus, it was necessary to verify whether a full performance recovery was possible by increasing the duration of the air interruption and for this reason, the same procedure was repeated after 24 hours (total 144 h), verifying that no further improvement was evident. This implies that a short exposure of the cathode catalyst to the potential of 0.20 V_{RHE} was not sufficient to achieve a full recovery. This suggested that full performance recovery could not be achieved by exclusively sweeping the potential, which is effective in removing oxides from the catalyst, but other phenomena governed by slower kinetics are suspected to play a role.

In the third approach, the cell was kept for 15 h with H_2 supplied to the anode at a rate of 50 mL min^{-1} and liquid water[10] supplied to the cathode at a rate of 0.3 mL min^{-1}. When the operation at 0.5 A cm^{-2} started again, a full performance recovery was observed. From this analysis, it is possible to conclude that under practical conditions PtOx formation contributes considerably to the recoverable performance loss, but this phenomenon does not explain it completely. Instead, it is possible to speculate a reversible Pt poisoning mechanism resulting from the interaction with the ionomer, which effect on ORR specific activity was demonstrated to be reversible, potential-dependent and related to active-site blockage [26–29]. The exact electrochemical mechanism was not identified yet to the authors' knowledge.

4. Conclusion

This work presented an experimental analysis of the recoverable performance loss in PEMFCs induced by PtOx formation, considering also the effect of aging. Three MEAs with different nanoparticle sizes and catalyst loadings were tested using EIS, constant-voltage, constant-current and potential controlled techniques. The analysis mainly focused on constant-voltage operation at 0.85 V in oxygen, which were suitable conditions for studying the oxide formation

[10] During the H_2/H_2O feeding the cathode potential was measured between 5 and 10 mV vs. RHE.

in the absence of mass-transport limitations. Different operating conditions, including low-voltage and constant-current operation with the air cathode were also investigated. The main conclusions of the presented research are as follows:

- During high voltage operation in fully humidified oxygen, PtOx formation is the main cause of the PEMFC recoverable performance loss. Most of the performance loss can be reversed by exposing cathode catalyst to low potential for short time.
- The evolution of specific ORR activity with time was found consistent for all studied MEAs, suggesting that recoverable performance decay is substantially unaffected by the nanoparticle growth induced by the AST.
- Linear sweep voltammetries reveal that surface oxide composition is influenced by catalyst morphology and modified by aging. However, an oxide associated with a stripping peak at around 0.61 V_{RHE} is always observed for all MEAs before and after aging.
- The relation between the PtOx coverage and specific ORR activity presents a common proportional behavior for all studied MEAs at both BOL and EOL. At specific activity equal to zero all the MEAs present a coverage (adopting a PtO basis) included between 0.55 and 0.65, suggesting the persistent presence of one type of oxide regardless of conditions and aging.
- The effect of PtOx on the recoverable performance loss is strongly influenced by the oxide composition. An increase in the coverage of the oxide associated with the peak at 0.61 V_{RHE} (obtained with a suitable cycling) impacts ORR activity more than an increase in the coverage of oxides formed at higher potentials.
- During constant-current operation in stack representative conditions, PtOx formation strongly contributes to the recoverable performance loss. A full performance recovery

can be obtained only over a long period (several hours) at a low cathode potential in presence of liquid water.

Acknowledgment

The authors acknowledge Matteo Bonanomi for support with the experimental measurements.

List of symbols

C_{DL}	Double layer capacitance (F m^{-3})
i^* ECSA	Volumetric exchange current density (A m^{-3})

Greek symbol

α	Transfer coefficient
φ	Porosity
σ	Ionic conductivity (S m^{-1})
δ	Thickness (μm)

Subscript

A	Relative to anode
C	Relative to cathode
M	Relative to membrane
CL	Relative to catalyst layer

Appendix A

Figure A.1 presents the LSVs performed after a 600 s voltage hold at 0.85 V in nitrogen, air and oxygen. The oxide reduction scans demonstrated the consistency of the surface oxide studied in a driven H_2/N_2 cell to fuel cell cathode operation.

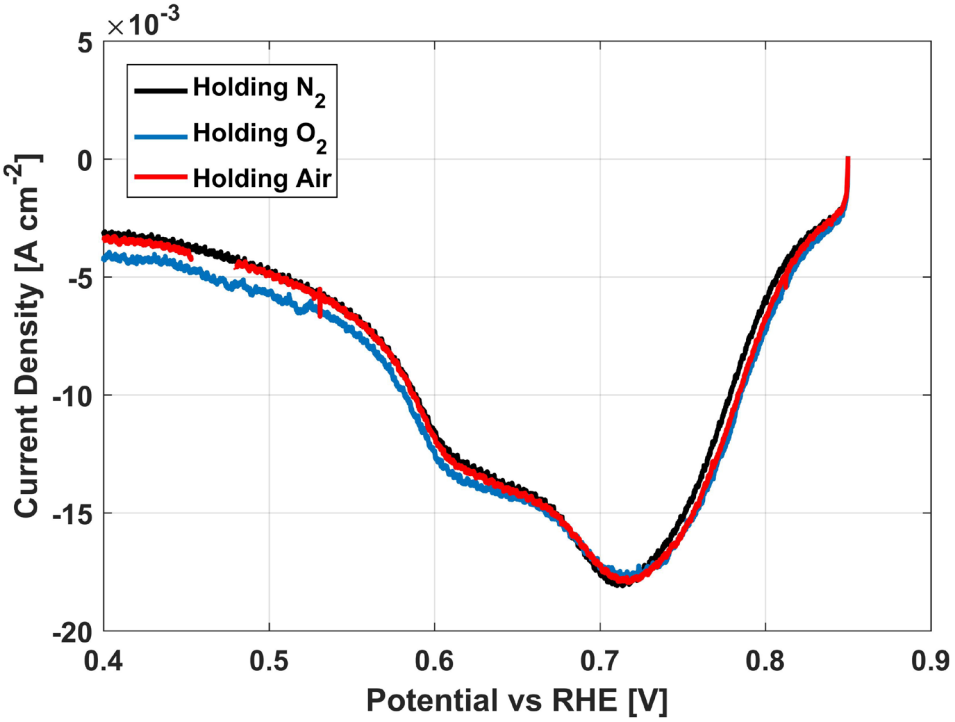

Fig. A.1 – LSVs performed after a 600 s potential hold at 0.85 V in N_2, air, and O_2.

Appendix B

Figure B.1 presents the simulated and measured Bode plots, before and after refresh, during the voltage hold at both 0.85 V and 0.70 V. The plots for the model and experiment agree well with each other, indicating that the main physical phenomena affecting cell performance have been reproduced correctly in the model.

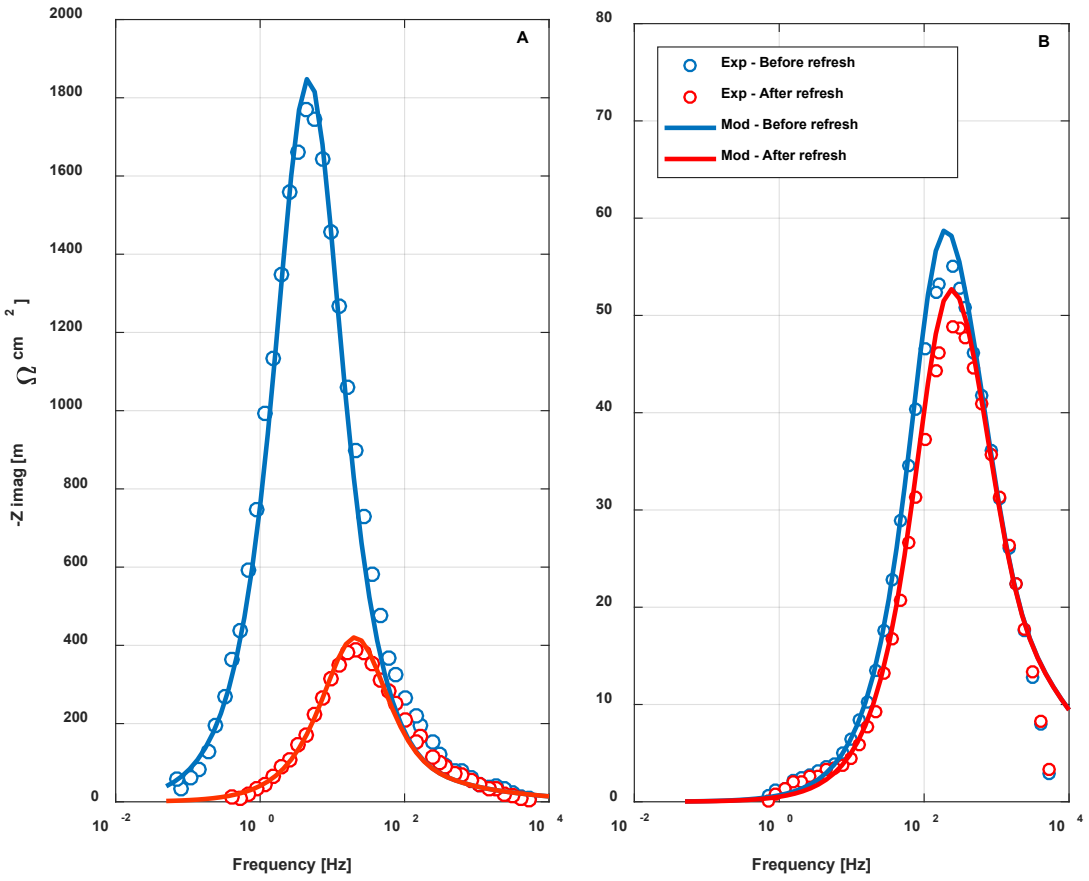

Fig. B.1 – Comparison between simulated and measured Bode plots before and after refresh: (A) voltage hold at 0.85 V; (B) voltage hold at 0.70 V.

References

[1] S.J.C. Cleghorn, D.K. Mayfield, D.A. Moore, J.C. Moore, G. Rusch, T.W. Sherman, N.T. Sisofo, U. Beuscher, A polymer electrolyte fuel cell life test: 3 years of continuous operation, J. Power Sources. 158 (2006) 446–454. doi:10.1016/j.jpowsour.2005.09.062.

[2] P. Gazdzick, J. Mitzel, D. Garcia Sanchez, M. Schulze, K.A. Friedrich, Evaluation of reversible and irreversible degradation rates of polymer electrolyte membrane fuel cells tested in automotive conditions, J. Power Sources. 327 (2016) 86–95. doi:10.1016/j.jpowsour.2016.07.049.

[3] J. Zhang, B.A. Litteer, F.D. Coms, R. Makharia, Recoverable Performance Loss Due to Membrane Chemical Degradation in PEM Fuel Cells, J. Electrochem. Soc. 159 (2012) F287–F293. doi:10.1149/2.063207jes.

[4] H. Li, Y. Tang, Z. Wang, Z. Shi, S. Wu, D. Song, J. Zhang, K. Fatih, J. Zhang, H. Wang, Z. Liu, R. Abouatallah, A. Mazza, A review of water flooding issues in the proton exchange membrane fuel cell, J. Power Sources. 178 (2008) 103–117. doi:10.1016/j.jpowsour.2007.12.068.

[5] F. a. Uribe, T. a. Zawodzinski, A study of polymer electrolyte fuel cell performance at high voltages. Dependence on cathode catalyst layer composition and on voltage conditioning, Electrochim. Acta. 47 (2002) 3799–3806. doi:10.1016/S0013-4686(02)00350-X.

[6] X. Yuan, H. Wang, J. Colin Sun, J. Zhang, Accelerate the Development and Introduction of Advanced Technologies Through Model Based System Engineering 2015, Int. J. Hydrogen Energy. 32 (2015) 4365–4380. doi:10.1016/j.ijhydene.2007.05.036.

[7] D.E. Ramaker, A. Korovina, V. Croze, J. Melke, C. Roth, Following ORR intermediates adsorbed on a Pt cathode catalyst during break-in of a PEM fuel cell by in operando X-ray absorption spectroscopy, Phys. Chem. Chem. Phys. 16 (2014) 13645–13653. doi:10.1039/C4CP00192C.

[8] R.K. Ahluwalia, S. Arisetty, J.-K. Peng, R. Subbaraman, X. Wang, N. Kariuki, D.J. Myers, R. Mukundan, R. Borup, O. Polevaya, Dynamics of Particle Growth and Electrochemical Surface Area Loss due to Platinum Dissolution, J. Electrochem. Soc. 161 (2014) F291–F304. doi:10.1149/2.051403jes.

[9] H. Baroody, Modelling oxide growth and formation on platinum, 144102 (2016).

[10] G. Jerkiewicz, G. Vatankhah, J. Lessard, M.P. Soriaga, Y.-S.S. Park, Surface-oxide growth at platinum electrodes in aqueous H2SO 4 Reexamination of its mechanism through combined cyclic-voltammetry, electrochemical quartz-crystal nanobalance, and Auger electron spectroscopy measurements, Electrochim. Acta. 49 (2004) 1451–1459. doi:10.1016/j.electacta.2003.11.008.

[11] J. Drnec, M. Ruge, F. Reikowski, B. Rahn, F. Carlà, R. Felici, J. Stettner, O.M. Magnussen, D.A. Harrington, Initial stages of Pt(111) electrooxidation: dynamic and structural studies by surface X-ray diffraction, Electrochim. Acta. 224 (2017) 220–227. doi:10.1016/j.electacta.2016.12.028.

[12] E.L. Redmond, B.P. Setzler, F.M. Alamgir, T.F. Fuller, Elucidating the oxide growth mechanism on platinum at the cathode in PEM fuel cells., Phys. Chem. Chem. Phys. 16 (2014) 5301–11. doi:10.1039/c3cp54740j.

[13] T. Nagai, H. Murata, Y. Morimoto, Analysis of the Relation between Oxidation State and ORR Activity of Pt by Linear Sweep Voltammetry, in: ECS Trans., 2010: pp. 125–130. doi:10.1149/1.3484509.

[14] H. Imai, K. Izumi, M. Matsumoto, Y. Kubo, K. Kato, Y. Imai, In Situ and Real-Time Monitoring of Oxide Growth in a Few Monolayers at Surfaces of Platinum Nanoparticles in Aqueous Media, J. Am. Chem. Soc. 131 (2009) 6293–6300. doi:10.1021/ja810036h.

[15] B.E. Conway, B. Barnett, H. Angerstein-Kozlowska, B. V. Tilak, A surface-electrochemical basis for the direct logarithmic growth law for initial stages of extension of anodic oxide

films formed at noble metals, J. Chem. Phys. 93 (1990) 8361. doi:10.1063/1.459319.

[16] B.E. Conway, ELECTROCHEMICAL AT NOBLE METALS OXIDE FILM FORMATION AS A SURFACE-CHEMICAL PROCESS, 49 (1995) 331–452.

[17] Y. Furuya, T. Mashio, A. Ohma, N. Dale, K. Oshihara, G. Jerkiewicz, Surface oxide growth on platinum electrode in aqueous trifluoromethanesulfonic acid, J. Chem. Phys. 141 (2014) 164705. doi:10.1063/1.4898707.

[18] K. Shinozaki, Y. Morimoto, B.S. Pivovar, S.S. Kocha, Re-examination of the Pt Particle Size Effect on the Oxygen Reduction Reaction for Ultrathin Uniform Pt/C Catalyst Layers without Influence from Nafion, Electrochim. Acta. 213 (2016) 783–790. doi:10.1016/j.electacta.2016.08.001.

[19] H. Yu, A. Baricci, A. Bisello, A. Casalegno, L. Guetaz, L. Bonville, R. Maric, Strategies to mitigate Pt dissolution in low Pt loading proton exchange membrane fuel cell: I. A gradient Pt particle size design, Electrochim. Acta. 247 (2017) 1155–1168. doi:10.1016/j.electacta.2017.07.093.

[20] A. Baricci, M. Zago, A. Casalegno, Modelling analysis of heterogeneity of ageing in high temperature polymer electrolyte fuel cells: insight into the evolution of electrochemical impedance spectra, Electrochim. Acta. 222 (2016) 596–607. doi:10.1016/j.electacta.2016.11.014.

[21] H. Yu, A. Baricci, A. Casalegno, L. Guetaz, L. Bonville, R. Maric, Strategies to mitigate Pt dissolution in low Pt loading proton exchange membrane fuel cell: II. A gradient Pt loading design, Electrochim. Acta. 247 (2017) 1169–1179. doi:10.1016/j.electacta.2017.06.145.

[22] H. Xu, R. Kunz, J.M. Fenton, Investigation of Platinum Oxidation in PEM Fuel Cells at Various Relative Humidities, Electrochem. Solid-State Lett. 10 (2007) B1. doi:10.1149/1.2372230.

[23] A. Baricci, M. Bonanomi, H. Yu, L. Guetaz, R. Maric, A. Casalegno, Modelling analysis of low platinum polymer fuel cell degradation under voltage cycling: Gradient catalyst layers with improved durability, J. Power Sources. 405 (2018) 89–100. doi:10.1016/J.JPOWSOUR.2018.09.092.

[24] M.J. Eslamibidgoli, J. Huang, T. Kadyk, A. Malek, M. Eikerling, How theory and simulation can drive fuel cell electrocatalysis, Nano Energy. 29 (2016) 334–361. doi:10.1016/j.nanoen.2016.06.004.

[25] D. Li, C. Wang, D.S. Strmcnik, D. V. Tripkovic, X. Sun, Y. Kang, M. Chi, J.D. Snyder, D. van der Vliet, Y. Tsai, V.R. Stamenkovic, S. Sun, N.M. Markovic, Functional links between Pt single crystal morphology and nanoparticles with different size and shape: the oxygen reduction reaction case, Energy Environ. Sci. 7 (2014) 4061–4069. doi:10.1039/C4EE01564A.

[26] K. Shinozaki, J.W. Zack, R.M. Richards, B.S. Pivovar, S.S. Kocha, Oxygen Reduction Reaction Measurements on Platinum Electrocatalysts Utilizing Rotating Disk Electrode Technique: I. Impact of Impurities, Measurement Protocols and Applied Corrections, J. Electrochem. Soc. 162 (2015) F1144–F1158. doi:10.1149/2.1071509jes.

[27] K. Kodama, A. Shinohara, N. Hasegawa, K. Shinozaki, R. Jinnouchi, T. Suzuki, T. Hatanaka, Y. Morimoto, Catalyst Poisoning Property of Sulfonimide Acid Ionomer on Pt (111) Surface, J. Electrochem. Soc. 161 (2014) F649–F652. doi:10.1149/2.051405jes.

[28] K. Kodama, K. Motobayashi, M. Osawa, R. Jinnouchi, A. Shinohara, T. Takeshita, Y. Morimoto, Voltammetric and Spectroscopic Analyses of the Effect of Ionomer on Oxygen Reduction Reaction on Pt Surface and Strategy for Developing Desirable Ionomers, Meet. Abstr. . MA2017-02 (2017) 1483.

[29] R. Subbaraman, D. Strmcnik, V. Stamenkovic, N.M. Markovic, Three Phase Interfaces at Electrified Metal - Solid Electrolyte Systems 1 . Study of the Pt (hkl) - Nafion Interface,

(2010) 8414–8422.